Classification using a two-qubit quantum chip

Niels M. P. Neumann

TNO, P.O. Box 96800, 2509JE The Hague, The Netherlands
niels.neumann@tno.nl

Abstract. Quantum computing has great potential for advancing machine learning algorithms beyond classical reach. Even though full-fledged universal quantum computers do not exist yet, its expected benefits for machine learning can already be shown using simulators and already available quantum hardware. In this work, we consider a distance-based classification algorithm and modify it to be run on actual early stage quantum hardware. We extend upon earlier work and present a non-trivial reduction using only two qubits. The algorithm is consequently run on a two-qubit silicon spin quantum computer. We show that the results obtained using the two-qubit silicon spin quantum computer are similar to the theoretically expected results.

Keywords: Classification · Machine learning · Quantum computing · Hardware implementations

1 Introduction

Whether we are aware of it or not, machine learning has taken a prominent role in our lives. For example, various algorithms are used to process text [1, 2] and speech [3, 4]. Furthermore, machine learning algorithms exist to recognise patterns [5] and also more specifically focused on recognising faces [6]. These are just a few of the many applications of machine learning.

In general, however, we can distinguish between three different types of machine learning: supervised, unsupervised and reinforced machine learning. In supervised machine learning, the machine is given annotated data, which is then used to train a model to annotate unseen data. Examples of supervised machine learning are decision trees, support vector machines and neural networks. Unsupervised machine learning algorithms use data without annotation and instead assign the labels themselves. Examples of unsupervised machine learning are clustering algorithms, such as k-means clustering. The third and last type is reinforced machine learning, or reinforcement learning, where a reward function is used that quantifies the 'goodness' of a solution. Based on the reward function, model parameters are adjusted. A prominent example of reinforcement learning applied in practice is AlphaGo, the first algorithm to beat a human at the game of Go [7]. As annotated data is in general expensive to gather, often a fourth type is considered: semi-supervised learning. Here a model is initially trained with a small set of annotated data, after which the rest of the learning is run unsupervised with a larger set of unlabeled data.

ICCS Camera Ready Version 2021
To cite this paper please use the final published version:
DOI: 10.1007/978-3-030-77980-1_6

Each of these types has its own challenges. Two common challenges across the four different types are however lack of data and intractability of the training phase, meaning that training the model is too complex. The intractability is often overcome by running the algorithms on (a clusters of) computers with more computational power. Instead, we may also opt for a completely different way of computing: doing computations using quantum computers. In quantum computers, computations are done using quantum bits (qubits) instead of classical bits. Classical bits are always in one of two possible definite states, zero or one. Qubits on the other hand can be in a superposition of the different computational basis states. A superposition is a complex linear combination of these states. Upon measurement a label corresponding to only one of the computational basis states is found. The probability to find each of the labels corresponds to the absolute value squared of the corresponding amplitudes. After the measurement, the state is projected onto a space corresponding to the found label and information on the initial superposition before the measurement is lost. Another key property of quantum states is that two qubits or, more general, multiple quantum states can be entangled. Entanglement implies correlations between two systems beyond what is possible classically. A more elaborated introduction to quantum computing is given in [8].

These quantum mechanical properties can be used to enhance classical computing and machine learning specifically [9, 10]. Quantum algorithms can for instance replace computationally expensive (sub)routines in classical algorithms, thereby enhancing the algorithm as a whole. Examples of computationally complex subroutines where quantum computing can offer benefits are sampling from probability distributions [11] and inverting matrices [12].

Another example of where quantum computing will provide improvements over classical algorithms is classification. In [13] for example, two quantum computing methods are proposed to classify data. The first method is a variational quantum classifier [14], similar to classical support vector machines (SVMs). In the second method, a kernel function is estimated and optimised directly. Instead of explicitly and iteratively training a machine learning model, a classifier can also be implemented directly from the data points, as in [15]. There, a controlled-SWAP-gate between the training data and a test data point is applied and two measurements are applied to classify the test data point. An example of distance-based classification is given in [16]. Here, a label is assigned based on a distance measure evaluated on the training points and a new test point. The classical complexity of this algorithm is $\mathcal{O}(NM)$, with N the number of data points and M the number of features. The time complexity of this quantum algorithm is constant, given efficient state preparation. The number of qubits n required is logarithmic in the number of data points, i.e., $n = \mathcal{O}(\log N)$.

For this constant complexity to hold, efficient state-preparation is a necessity. This can however pose challenges [17], and, if the state is prepared explicitly, even can result in an exponential overhead in the number of qubits. In general, an $m \times m$-qubit unitary gate can be decomposed exactly in $\mathcal{O}(m^3 4^m)$ single qubit and CNOT-gates [18], which was later reduced to $\mathcal{O}(2^m)$ quantum gates [19, 20].

ICCS Camera Ready Version 2021
To cite this paper please use the final published version:
DOI: 10.1007/978-3-030-77980-1_6

Instead of explicit state preparation, the state can also be obtained from the output of other quantum processes or by using a quantum RAM [21], a register or quantum computer that stores specific states. Note that for the latter, the challenge shifts from efficiently preparing a quantum state to efficiently preparing and storing the states in the quantum RAM. An approach proposed in [22] uses a divide-and-conquer algorithm for quantum state preparation, with a poly-logarithmic complexity in N, the number of data points, compared to a classical complexity of $\mathcal{O}(N)$. The complexity of the quantum distance-based classifier of [16] thus depends on the complexity of state-preparation.

Especially for near-term devices with limited resources, state preparation can limit the applicability of this algorithm. A reduction to overcome this limitation is presented in [23]. By formulating the algorithm as a quantum channel and considering a single data point at a time, similar performance is reached as with the original algorithm. Conditional on the measurement of the ancilla qubit either a new data point is chosen uniformly at random or the label is assigned to the test point. We consider a different non-trivial reduction of the distance-based classifier to be run on near-term hardware, classifying data points in one of two classes. Our algorithm can be used as benchmarking algorithm for comparison with classical devices and to compare different quantum chips. In this work, we compare the classical theoretical results with the results obtained through a decoherence-free quantum simulation and by running the algorithm on a two-qubit silicon spin quantum chip developed by QuTech. In Section 2 we briefly explain the distance-based classifier presented in [16]. In Section 3 we present a non-trivial reduction of the algorithm to a two-qubit version. The results of running the algorithm on the quantum hardware and on the simulator are presented and compared to the theoretically expected results in Section 4. Conclusions are given in Section 5.

2 Distance-based classifier

In this section we explain the quantum distance-based classifier proposed in [16]. This algorithm classifies a test point, based on its distances to data points in a data set. The algorithm returns a binary variable representing the label of the test point.

Consider a data set $\mathcal{D} = \{\mathbf{x}^i, y^i\}_{i=0}^{N-1}$ with data points $\mathbf{x}^i \in \mathbb{R}^M$ and labels $y^i \in \{\pm 1\}$. Let $\tilde{\mathbf{x}} \in \mathbb{R}^M$ be an unlabeled data point, the goal is to assign the label $\tilde{y}$ to this data point $\tilde{\mathbf{x}}$. The algorithm presented in [16], implements the threshold function

$$\tilde{y} = \operatorname{sgn}\left(\sum_{i=0}^{N-1} y^i \left[1 - \frac{1}{4N}\left\|\tilde{\mathbf{x}} - \mathbf{x}^i\right\|^2\right]\right), \tag{1}$$

where $\operatorname{sgn}\colon \mathbb{R} \to \{-1, 1\}$ is the signum function and $\kappa(\tilde{\mathbf{x}}, \mathbf{x}) = 1 - \frac{1}{4N}\left\|\tilde{\mathbf{x}} - \mathbf{x}\right\|^2$ is the similarity function or kernel.

ICCS Camera Ready Version 2021
To cite this paper please use the final published version:
DOI: 10.1007/978-3-030-77980-1_6

Without loss of generality we can assume that the data points in $\mathcal{D}$ are normalised. The data points can then be encoded in qubits:

$$\mathbf{x} = (x_0, \ldots, x_{M-1})^T \mapsto |\mathbf{x}\rangle = \sum_{j=0}^{M-1} x_j \, |j\rangle \,,$$

with x_j the j-th coefficient of $\mathbf{x}$ and $|j\rangle$ the j-th computational basis state. Let us consider the quantum state

$$|\mathcal{D}\rangle = \frac{1}{\sqrt{2N}} \sum_{i=0}^{N-1} |i\rangle \left(|0\rangle \, |\tilde{\mathbf{x}}\rangle + |1\rangle \, |\mathbf{x}^i\rangle \right) |y^i\rangle \,. \tag{2}$$

Here, the first register $|i\rangle$ is an index register, indexing the data points. The second register is an ancilla qubit entangled with the test point and the i-th data point. The fourth register encodes the label y^i. In case of only two classes, the fourth register is only a single qubit. Note that binary labels y and labels $s \in \{\pm 1\}$ are directly related via $y = (s+1)/2$.

The algorithm starts from the quantum state of Eq. (2) and consists of a Hadamard operation on the ancilla qubit, a measurement of that qubit and a measurement of the fourth register. Due to the probabilistic nature of quantum algorithms, multiple measurement rounds should be used. The label of the test point is assigned based on the measurement of the fourth register, conditional on the first measurement giving a 0. Results where the first measurement gives a 1 should be neglected.

After the Hadamard gate we are left with

$$|\mathcal{D}\rangle = \frac{1}{2\sqrt{N}} \sum_{i=0}^{N-1} |i\rangle \left(|0\rangle \left(|\tilde{\mathbf{x}}\rangle + |\mathbf{x}^i\rangle \right) + |1\rangle \left(|\tilde{\mathbf{x}}\rangle - |\mathbf{x}^i\rangle \right) \right) |y^i\rangle \,. \tag{3}$$

Measuring the ancilla qubit and only continuing with the algorithm if the $|0\rangle$-state is measured, leaves us with

$$|\mathcal{D}\rangle = \frac{1}{2\sqrt{N p_{acc}}} \sum_{i=0}^{N-1} |i\rangle \, |0\rangle \left(|\tilde{\mathbf{x}}\rangle + |\mathbf{x}^i\rangle \right) |y^i\rangle \,. \tag{4}$$

Here, p_{acc} is the probability of measuring 0, given by

$$p_{acc} = \frac{1}{4N} \sum_i \left\| \tilde{\mathbf{x}} + \mathbf{x}^\mathbf{i} \right\|^2 . \tag{5}$$

If instead the $|1\rangle$-state is measured, the algorithm should be aborted and run again, which can also be taken care of in a post-processing step. The probability of obtaining a label $\tilde{y} = 1$ is given by

$$\mathbb{P}(\tilde{y} = 1) = \frac{1}{4N p_{acc}} \sum_{i | y^i = 1} \left\| \tilde{\mathbf{x}} + \mathbf{x}^i \right\|^2 . \tag{6}$$

ICCS Camera Ready Version 2021
To cite this paper please use the final published version:
DOI: 10.1007/978-3-030-77980-1_6

If both classes have the same number of data points and the data points are normalised, we have

$$\frac{1}{4N}\sum_i \left\|\tilde{\mathbf{x}}+\mathbf{x}^i\right\|^2 = 1-\frac{1}{4N}\sum_i \left\|\tilde{\mathbf{x}}-\mathbf{x}^i\right\|^2.$$

Therefore, the algorithm implements the classifier of Eq. (1). By evaluating the algorithm multiple times, the most likely class is obtained.

Note that, as discussed in the introduction, the constant complexity of this algorithm is under the assumption of efficient state preparation, for instance using a quantum RAM. Extensions on this work and relaxation of assumptions in the original work are given in [24]. One of these assumptions is that all classes contain the same number of data points. In the next section we will reduce this distance-based classifier to a two qubit version.

3 Reduction to a two-qubit version

In this section we present a non-trivial reduction of the distance-based classifier to a two qubit version to be run on few qubit quantum hardware. This reduced algorithm can consequently be used for comparing the fidelity of pairs of qubits due to the simple nature of this algorithm. The algorithm proposed in this section produces the same probability distribution for the measured labels as the original distance-based classifier for a given data set. In our approach, we use the same qubit for both encoding the data points as well as encoding the labels.

For a two-qubit version of the algorithm, we consider a training set $\mathcal{D} = \{(\mathbf{x}^0,-1),(\mathbf{x}^1,1)\}$ and a test point $\tilde{\mathbf{x}}$, with each data point having two features. We can encode the data points as

$$\begin{aligned}
|\mathbf{x}^0\rangle &= \cos(\theta/2)\,|0\rangle - \sin(\theta/2)\,|1\rangle\\
|\mathbf{x}^1\rangle &= \cos(\phi/2)\,|0\rangle - \sin(\phi/2)\,|1\rangle\\
|\tilde{\mathbf{x}}\rangle &= \cos(\omega/2)\,|0\rangle - \sin(\omega/2)\,|1\rangle\,,
\end{aligned}$$

such that $R_y(\theta)\,|0\rangle = |\mathbf{x}^0\rangle$. Without loss of generality we may assume $\theta = 0$. Furthermore, note that for two data points, the index register and the label register have the same value. Hence, the two can be combined and the initial state is given by

$$\begin{aligned}
&\frac{1}{2}\,|0\rangle\left(\,|0\rangle\,|\tilde{\mathbf{x}}\rangle + |1\rangle\,|0\rangle\,\right)\\
+&\frac{1}{2}\,|1\rangle\left(\,|0\rangle\,|\tilde{\mathbf{x}}\rangle + |1\rangle\,|\mathbf{x}^1\rangle\,\right).
\end{aligned}$$

The ratio of the probabilities when measuring the first register is then given by

$$\frac{\mathbb{P}(|y^i\rangle = |0\rangle)}{\mathbb{P}(|y^i\rangle = |1\rangle)} = \frac{\cos^2\left(\frac{\omega}{4}\right)}{\cos^2\left(\frac{\omega-\phi}{4}\right)}, \tag{7}$$

ICCS Camera Ready Version 2021
To cite this paper please use the final published version:
DOI: 10.1007/978-3-030-77980-1_6

with ω and ϕ depending on the data points. For a further reduction to only two qubits we set $t = \cos^2\left(\frac{\omega}{4}\right) / \cos^2\left(\frac{\omega-\phi}{4}\right)$, and define

$$\omega' = \begin{cases} 4\arctan\left(\frac{1-\sqrt{t}}{1+\sqrt{t}}\right) & \text{if } t \neq 1 \\ 0 & \text{else} \end{cases}. \tag{8}$$

For $t = 1$ both classes are equally likely. We propose the quantum circuit shown in Fig. 1 for classification. The resulting probability distribution is equal to that of the original classifier.

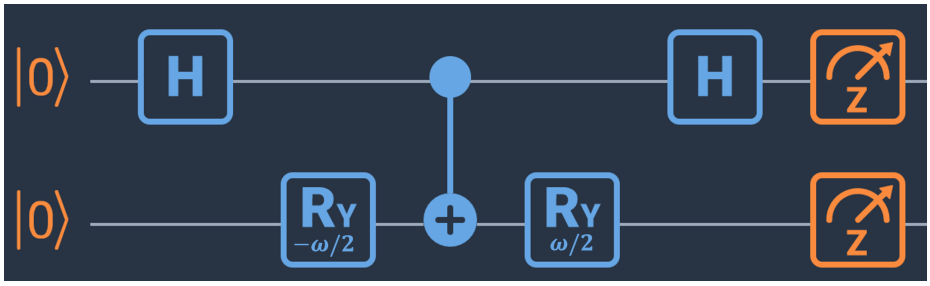

Fig. 1. A two qubit classification quantum circuit. The operations are a Hadamard gate (H), rotations around the Y-axis (R_y), a controlled-NOT operation ($CNOT$) and two measurements. The used angle depends on the data points.

The quantum circuit in Fig. 1 produces the desired probability distributions. The first gates prepare the desired quantum state and the last Hadamard-gate is similar to the operation in the original algorithm. The initial state is given by

$$\frac{1}{\sqrt{2}}\left(\cos(\omega'/2)\,|00\rangle + \sin(\omega'/2)\,|01\rangle + |11\rangle\right) \tag{9}$$

and the quantum state before the measurements is

$$\begin{aligned} &\frac{1}{2}\left(\cos(\omega'/2)\,|00\rangle + \cos(\omega'/2)\,|10\rangle\right. \\ &\left. + \left(1+\sin(\omega'/2)\right)|01\rangle + \left(1-\sin(\omega'/2)\right)|11\rangle\right). \end{aligned}$$

When measuring the first (left-most) qubit and only continuing if the $|0\rangle$-state is measured, we have

$$\frac{1}{2\sqrt{p'_{acc}}}\left(\cos(\omega'/2)\,|00\rangle + \left(1+\sin(\omega'/2)\right)|01\rangle\right), \tag{10}$$

with p'_{acc} the acceptance probability given by

$$p'_{acc} = \frac{1+\sin(\omega'/2)}{2}. \tag{11}$$

ICCS Camera Ready Version 2021
To cite this paper please use the final published version:
DOI: 10.1007/978-3-030-77980-1_6

Note that this acceptance probability differs from the one given in Eq. (5), however the conditional probabilities of measuring the labels does match that of the original algorithm. This acceptance probability only depends on the distribution of the considered data points on the unit circle.

The method above can be generalised to arbitrary data sets with two classes. Instead of a single data point, a representative of each data set is used in the classification. This follows as for normalised data, only the angle of the data point is considered and each angle has an equal contribution. Hence, the mean of the angles can be used for the representative data point. This step requires the computation of two means, both of $N/2$ angles.

4 Results

In this section we present the results when running the algorithm on quantum hardware and on a quantum simulator. These results are compared to the results we expect based on a theoretical evaluation of the quantum operations. These expected probabilities are obtained from the quantum state in Eq. (10) and the acceptance probability from Eq. (11).

We used the Quantum Inspire platform [25, 26], developed by QuTech, to obtain our results. This online platform hosts two quantum chips: a 2-qubit silicon spin chip and a 5-qubit transmon chip. Furthermore, a quantum simulator based on the QX programming language is available [27]. We used the publicly available 2-qubit silicon spin chip for our results.

For the experiments we use the Iris flower data set [28]. This data set contains 150 data points, equally distributed over three classes. Each data point has four features. We only consider the Setosa and Versicolor class and the first two features of the data points: the width and length of the sepal leaves. We standardise and normalise the data points and then randomly sample data points to form the data sets to run the algorithm with. Additionally, we randomly sample another data point, not used yet, together with its corresponding label. This data point is used as test point. For the first data set, we sample the test point from the Setosa class, for the second data set we sample the test point from the Versicolor class. The three data points of each data set can now be written as

$$\begin{aligned} |\mathbf{x}^0\rangle &= |0\rangle \\ |\mathbf{x}^1\rangle &= \cos(\phi/2)\,|0\rangle - \sin(\phi/2)\,|1\rangle \\ |\tilde{\mathbf{x}}\rangle &= \cos(\omega/2)\,|0\rangle - \sin(\omega/2)\,|1\rangle\,, \end{aligned}$$

with appropriate angles ϕ and ω. We identify label 0 with the Setosa class and label 1 with the Versicolor class.

For the first data set we have $\mathbf{x}^0 = (1, 0)$, $\mathbf{x}^1 = (-0.9929, 0.1191)$ and $\tilde{\mathbf{x}} = (0.9939, 0.1103)$, which correspond with Iris samples 34, 75 and 13, respectively. The corresponding angles are $\phi \approx -6.0445$ and $\omega \approx -0.2210$. For the second data set we randomly chose Iris samples 21, 58 and 82. Hence, the data points

ICCS Camera Ready Version 2021
To cite this paper please use the final published version:
DOI: 10.1007/978-3-030-77980-1_6

are given by $\mathbf{x}^0 = (1, 0)$, $\mathbf{x}^1 = (-0.1983, 0.9802)$ and $\tilde{\mathbf{x}} = (0.5545, 0.8322)$. The corresponding angles are $\phi \approx -3.5407$ and $\omega \approx -1.9662$. Both data sets are shown in Figure 2. Based on a visual inspection, the first data set should be easier to correctly classify than the second.

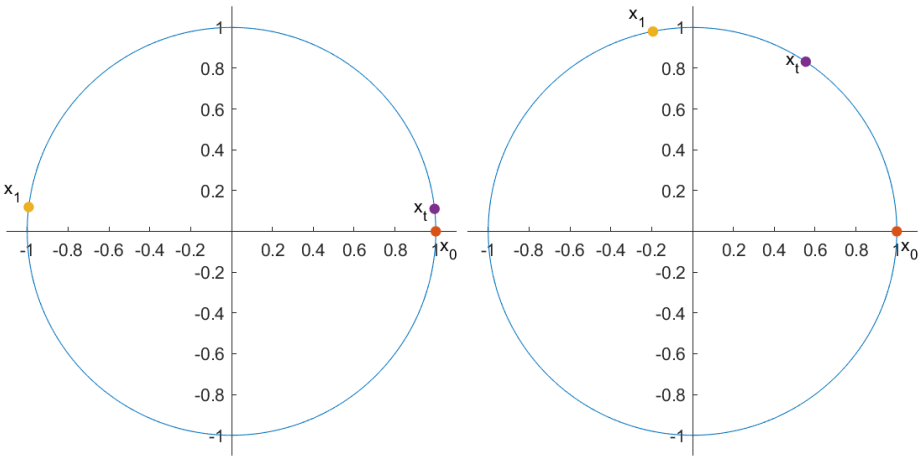

Fig. 2. Data set 1 (left) and data set 2 (right) used for the experiments. The label indicates the data points. The test point is given by x_t.

For both data sets, we determine t and ω' and consequently run the circuit as shown in Fig. 1 on the quantum simulator and on the 2-qubit silicon spin chip with 2,048 circuit evaluations in total. Additionally, we present the theoretically expected probabilities, which correspond with an infinite number of evaluations. The found probabilities are shown in Tab. 1 and the different between the simulation results and the theoretical results are due to the finite number of shots for the simulations. This table also shows the acceptance probabilities. The shown probabilities for both labels are conditional on the ancilla qubit being in the $|0\rangle$-state.

We see a significant different between the acceptance probability for both data sets. This results from the initial distribution of the data points on the unit circle. Different acceptance probabilities are expected for different initial distributions. For the second data set, the probabilities corresponding to both classes matches well with the expected probabilities. For the first data set, the probabilities differ more, likely due to decoherence effects. Note that in all cases, the correct label is assigned to the test point: label 0 for the first data set and label 1 for the second data set.

ICCS Camera Ready Version 2021
To cite this paper please use the final published version:
DOI: 10.1007/978-3-030-77980-1_6

Table 1. Shown are the results for classifying $\tilde{\mathbf{x}}$. Hardware and simulation results are shown as well as the theoretical values. The results hardware and simulation results are taken from 2048 measurement rounds.

		p_{acc}	$\mathbb{P}(y^m) = -1$	$\mathbb{P}(y^m) = 1$
Data set 1	Hardware	0.83544	0.7744	0.2256
	Simulation	0.9893	0.9877	0.0123
	Theoretical	0.9870	0.9870	0.0130
Data set 2	Hardware	0.3755	0.4655	0.5345
	Simulation	0.4863	0.4719	0.5281
	Theoretical	0.5232	0.4768	0.5232

5 Conclusions

This paper presented a non-trivial reduction of the distance-based classification algorithm of [16] to a two qubit version. Due to the simple nature of the reduced algorithm, it can be used to compare various near-term quantum chips with limited number of qubits. Different quantum chips can be compared based on how close the found results are to the expected ones. In this work we considered the two qubit silicon spin chip developed by QuTech and modified the algorithm to be run on that hardware backend. The algorithm classifies a data point in one of two classes. Due to the limited size, the classes are represented as single data points. Classification using larger data sets is still possible by considering the single data point used in the algorithm as being a representative of the entire class. Thereby, arbitrarily sized data sets can be used, after a suitable preprocessing step.

The obtained probability distributions are similar to the theoretically expected results, however with the differences resulting from decoherence and different rotation angles. For small rotation angles, the probability of introducing errors is also smaller. We found that the same probability distribution is produced as one would obtain with the original multi-qubit approach, however, less qubits are used. We tested the algorithm with two random data sets and in both cases, the correct label was assigned to the test point. The hardware used to produce these results was a two-qubit silicon spin quantum chip, developed by QuTech and hosted publicly on the Quantum Inspire platform.

6 Acknowledgements

This work is the result of the quantum technology project of TNO. There are no conflict of interests for the authors.

References

1. A. C. R. Hogervorst, M. K. van Dijk, P. C. M. Verbakel, and C. Krijgsman, "Handwritten character recognition using neural networks," in *Neural Networks: Artificial*

ICCS Camera Ready Version 2021
To cite this paper please use the final published version:
DOI: 10.1007/978-3-030-77980-1_6

Intelligence and Industrial Applications (B. Kappen and S. Gielen, eds.), (London), pp. 337–343, Springer London, 1995.
2. K. I. Kim, K. Jung, S. H. Park, and H. J. Kim, "Support vector machines for texture classification," *IEEE Transactions on Pattern Analysis and Machine Intelligence*, vol. 24, no. 11, pp. 1542–1550, 2002.
3. A. Graves, A. Mohamed, and G. Hinton, "Speech recognition with deep recurrent neural networks," in *2013 IEEE International Conference on Acoustics, Speech and Signal Processing*, pp. 6645–6649, 2013.
4. O. Abdel-Hamid, A. Mohamed, H. Jiang, L. Deng, G. Penn, and D. Yu, "Convolutional neural networks for speech recognition," *IEEE/ACM Transactions on Audio, Speech, and Language Processing*, vol. 22, no. 10, pp. 1533–1545, 2014.
5. C. M. Bishop, *Pattern Recognition and Machine Learning*. Springer, 2006.
6. S. Lawrence, C. L. Giles, Ah Chung Tsoi, and A. D. Back, "Face recognition: a convolutional neural-network approach," *IEEE Transactions on Neural Networks*, vol. 8, no. 1, pp. 98–113, 1997.
7. D. Silver, A. Huang, C. J. Maddison, A. Guez, L. Sifre, G. van den Driessche, J. Schrittwieser, I. Antonoglou, V. Panneershelvam, M. Lanctot, S. Dieleman, D. Grewe, J. Nham, N. Kalchbrenner, I. Sutskever, T. Lillicrap, M. Leach, K. Kavukcuoglu, T. Graepel, and D. Hassabis, "Mastering the game of go with deep neural networks and tree search," *Nature*, vol. 529, p. 484–489, Jan 2016.
8. M. A. Nielsen and I. L. Chuang, *Quantum Computation and Quantum Information: 10th Anniversary Edition*. Cambridge University Press, 2010.
9. M. Schuld, I. Sinayskiy, and F. Petruccione, "An introduction to quantum machine learning," *Contemporary Physics*, vol. 56, no. 2, pp. 172–185, 2015.
10. N. M. P. Neumann, F. Phillipson, and R. Versluis, "Machine learning in the quantum era," *Digitale Welt*, vol. 3, pp. 24–29, 4 2019.
11. A. Perdomo-Ortiz, M. Benedetti, J. Realpe-Gómez, and R. Biswas, "Opportunities and challenges for quantum-assisted machine learning in near-term quantum computers," *Quantum Science and Technology*, vol. 3, p. 030502, Jun 2018.
12. A. W. Harrow, A. Hassidim, and S. Lloyd, "Quantum algorithm for linear systems of equations," *Phys. Rev. Lett.*, vol. 103, p. 150502, Oct 2009.
13. V. Havlíček, A. D. Córcoles, K. Temme, A. W. Harrow, A. Kandala, J. M. Chow, and J. M. Gambetta, "Supervised learning with quantum-enhanced feature spaces," *Nature*, vol. 567, pp. 209–212, mar 2019.
14. K. Mitarai, M. Negoro, M. Kitagawa, and K. Fujii, "Quantum circuit learning," *Phys. Rev. A*, vol. 98, p. 032309, Sep 2018.
15. D. K. Park, C. Blank, and F. Petruccione, "The theory of the quantum kernel-based binary classifier," *Physics Letters A*, vol. 384, no. 21, p. 126422, 2020.
16. M. Schuld, M. Fingerhuth, and F. Petruccione, "Implementing a distance-based classifier with a quantum interference circuit," *EPL (Europhysics Letters)*, vol. 119, p. 60002, Sep 2017. arXiv: 1703.10793.
17. S. Aaronson, "Read the fine print," *Nature Physics*, vol. 11, p. 291–293, Apr 2015.
18. A. Barenco, C. H. Bennett, R. Cleve, D. P. DiVincenzo, N. Margolus, P. Shor, T. Sleator, J. A. Smolin, and H. Weinfurter, "Elementary gates for quantum computation," *Phys. Rev. A*, vol. 52, pp. 3457–3467, Nov 1995.
19. M. Möttönen, J. J. Vartiainen, V. Bergholm, and M. M. Salomaa, "Transformation of quantum states using uniformly controlled rotations," *Quantum Inf. Comput.*, vol. 5, no. 6, pp. 467–473, 2005.
20. V. V. Shende, S. S. Bullock, and I. L. Markov, "Synthesis of quantum-logic circuits," *IEEE Transactions on Computer-Aided Design of Integrated Circuits and Systems*, vol. 25, no. 6, pp. 1000–1010, 2006.

ICCS Camera Ready Version 2021
To cite this paper please use the final published version:
DOI: 10.1007/978-3-030-77980-1_6

21. V. Giovannetti, S. Lloyd, and L. Maccone, "Quantum random access memory," *Phys. Rev. Lett.*, vol. 100, p. 160501, Apr 2008.
22. I. F. Araujo, D. K. Park, F. Petruccione, and A. J. da Silva, "A divide-and-conquer algorithm for quantum state preparation," *Scientific Reports*, vol. 11, mar 2021.
23. P. Sadowski, "Quantum distance-based classifier with distributed knowledge and state recycling," *International Journal of Quantum Information*, vol. 16, p. 1840013, Dec. 2018.
24. R. Wezeman, N. Neumann, and F. Phillipson, "Distance-based classifier on the quantum inspire," *Digitale Welt*, vol. 4, p. 85–91, Jan 2020.
25. QuTech, "Quantum inspire." https://www.quantum-inspire.com, 2020.
26. T. Last, N. Samkharadze, P. Eendebak, R. Versluis, X. Xue, A. Sammak, D. Brousse, K. Loh, H. Polinder, G. Scappucci, M. Veldhorst, L. Vandersypen, K. Maturová, J. Veltin, and G. Alberts, "Quantum Inspire: QuTech's platform for co-development and collaboration in quantum computing," in *Novel Patterning Technologies for Semiconductors, MEMS/NEMS and MOEMS 2020* (M. I. Sanchez and E. M. Panning, eds.), vol. 11324, pp. 49 – 59, International Society for Optics and Photonics, SPIE, 2020.
27. N. Khammassi, I. Ashraf, X. Fu, C. G. Almudever, and K. Bertels, "QX: A high-performance quantum computer simulation platform," in *Design, Automation Test in Europe Conference Exhibition (DATE), 2017*, pp. 464–469, 2017.
28. R. A. Fisher, "The use of multiple measurements in taxonomic problems," *Annual Eugenics*, vol. 7, pp. 179–188, 1936.

ICCS Camera Ready Version 2021
To cite this paper please use the final published version:
DOI: 10.1007/978-3-030-77980-1_6